Electronic bond rupture of Si atoms on Si(111)-(2×1) induced by valence excitation

E. Inami and K. Tanimura
The Institute of Scientific and Industrial Research, Osaka University, 8-1 Mihoga-oka, Ibaraki, Osaka 567-0047, Japan
(Received 11 April 2007; published 12 July 2007)

Scanning tunneling microscopy study reveals the electronic local bond rupture of threefold-coordinated Si atoms at intrinsic sites on Si(111)-(2×1) under nanosecond-laser excitation at 1064 nm. The rate of bond rupture leading to monovacancy formation on the surface depends superlinearly on the excitation intensity. This primary step of surface-structural change is followed by efficient formation of vacancy clusters with two distinctive morphologies: vacancy strings aligned along the Si-atom chain in one dimension and vacancy islands developed across the chains in two dimensions. Quantitative analysis of the vacancy clustering process shows that the bond-rupture rate at sites nearest to pre-existing surface defects is enhanced more than a factor of 1000 relative to perfect sites. We also studied effects of different excitation wavelength and of Fermi-level positions on the bond-rupture process. The laser-induced surface bond-rupture mechanism is discussed in terms of two-hole localization of optically generated nonequilibrated valence holes on the surface sites.

DOI: 10.1103/PhysRevB.76.035311 PACS number(s): 79.20.La, 68.37.Ef, 61.80.Ba, 68.35.Bs

I. INTRODUCTION

Laser interaction with semiconductor surfaces has been studied extensively motivated by interest in both applied and basic research into light-matter interactions. By combining direct atomic imaging of the irradiated surfaces using scanning tunneling microscopy[1–8] (STM) with high-sensitivity detection of neutral desorbed species using postionization techniques,[4,8–11] recent studies have demonstrated the crucial roles of electronic processes in the surface bond rupture and desorption of constituent atoms. The excitation-induced structural instability leads to drastic structural changes and shows some important common features over several semiconductor surfaces with different structures and electronic properties. First, atoms at perfect surface sites are subject to bond rupture, thus showing an intrinsic nature of these processes. Secondly, ground-state neutral atoms are desorbed, not ions. Finally, the rates of bond rupture depend superlinearly on the excitation-laser intensity.

However, significant differences have been revealed in the morphologies of the induced structural changes and in the excitation-wavelength dependence on the bond-rupture rates. For example, monovacancies are almost exclusively formed on Si(111)-(7×7) up to the surface monovacancy concentration of a few percent,[4] while efficient clustering of surface vacancies is induced on (110)-(1×1) surfaces of InP and GaAs.[7] The bond-rupture rate is resonantly enhanced at an excitation-photon energy of 2 eV for Si(111)-(7×7),[4] while a rather broad range of excitation wavelengths can induce bond rupture with similar rates for InP(110)-(1×1).[7] More systematic and extensive studies of other typical surfaces are desirable in establishing the general bond-breaking mechanism.

The Si(111)-(2×1) surface, formed upon cleavage in ultrahigh vacuum (UHV), is one of the best understood reconstructed surfaces.[12,13] The surface structure is characterized by quasi-one-dimensional zigzag chains of Si, accompanied by a substantial buckling of the topmost chains. The buckling is associated with a significant ionicity induced by a net charge transfer from the down Si atoms (Si_{down}) to the up Si atoms (Si_{up}).[14–17] The structural and electronic properties of Si(111)-(2×1), characterized by quasi-one-dimensional chains and strong bond ionicity, are significantly different from those of Si(111)-(7×7) and Si(001)-(2×1), but similar to those of (110) surfaces of III-V compound semiconductors.[12]

Since the excitation-induced instability is surface specific for semiconductors, it is clear that charge redistribution on surfaces, induced by generation and relaxation of surface excited states, plays a crucial role in the instability. Surface excited species can be populated by two different channels: direct surface-specific optical excitation and indirect electronic excitation transfer from bulk to surface states. Since optical-transition energies between surface electronic states are overlapped with those of bulk-electronic states in most cases,[12] both channels can be active under excitation at a given photon energy, making it more difficult to delineate the primary processes. The Si(111)-(2×1) surface has a property which is advantageous for separating surface and bulk optical transitions. Surface optical spectroscopy studies[18,19] have shown the prominent optical absorption peak at 0.46 eV that originates from transitions at the minimum surface band gap between the dangling-bond bands. The absorption coefficient of the surface band decreases to nearly zero above 1.0 eV. There are other surface optical-transition bands between 1.2 and 3.5 eV. These surface-specific optical transitions give the least contribution around 1.1 eV, where bulk-valence transitions become possible; the band gap energy of Si is 1.11 eV at 300 K.[20] By carefully tuning the photon excitation energy near 1.1 eV, bulk or surface excitation may be induced preferentially.

In this paper, we study the surface-structural changes of Si(111)-(2×1), induced by 1064 nm (1.16 eV) excitation. Direct imaging of atomic structures by STM shows that the monovacancy formation at perfect surface site is the primary step, followed by efficient formation of vacancy clusters. The dependency of the bond-rupture rates on the excitation density, excitation wavelength, and sample Fermi level is also studied. The characteristic features of the instability can be analyzed satisfactorily by the mechanism of two-hole local-

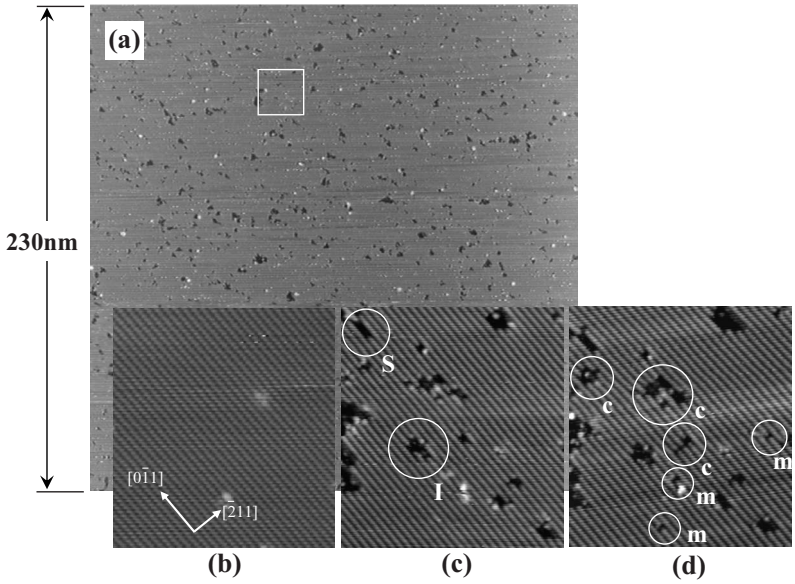

FIG. 1. STM images acquired with a negative sample-bias voltage of −2.5 V for Si(111)-(2×1). Image (a) is a wide view of 0.23 ×0.23 μm^2 of the surface irradiated with 5000 shots of laser pulses to show a wide terrace without any steps. Images (b), (c), and (d) show a magnified view of the area indicated by the white rectangle in (a), before (b), after 5000 laser pulses (c), and after 20 000 laser pulses (d), with 1064 nm laser pulses at fluence of 30 mJ cm^{-2}. For symbols in (c) and (d), see the text.

ization (THL) of the optically generated nonequilibrated valence holes.

II. EXPERIMENT

Crystals used were P-doped ($\sim 3\times 10^{15}$ cm^{-3}) *n*-type Si with the resistivity ρ of 3.15 Ω cm and B-doped ($\sim 2\times 10^{16}$ cm^{-3}) *p*-type Si with ρ of 1.25 Ω cm. Specimens with a cross section of 0.2×5 mm^2 were cleaved in a UHV chamber with a base pressure of 5×10^{-11} Torr, and the structures were characterized by using a UHV-STM system (UNISOKU STM-U2) at 296 K. Laser pulses of 1064 nm (3.5 ns width), generated with an yttrium aluminum garnet laser (Coherent, Infinity) with 10 Hz repetition rate, were used to excite the surface with the incident angle of 45°. The laser beam was focused on the surface by a quartz lens. The beam profile on the surface was described well by a Gaussian with a full width at half maximum of 0.2 mm. The intensities of the laser pulses were controlled by putting neutral density filters in the optical path and were monitored by directing a portion of the beam reflected by a quartz plate to a calibrated photodiode (Hamamatsu, model S1337-1010BQ).

III. RESULTS

Figure 1 represents STM images acquired before and after irradiation with 1064 nm laser pulses at a fluence of 30 mJ cm^{-2} (the intensity of 8.6 MW cm^{-2}). Image (a) shows a wide view of the surface irradiated with 5000 laser pulses. The surface is characterized by a single domain terrace as wide as 0.23×0.23 μm^2. The area, indicated by a white rectangle in Fig. 1(a), is shown in expanded scale in images (b), (c), and (d). In image (b), which represents the surface prior to laser excitation, each white spot corresponds to the Si_{up}, and quasi-one-dimensional rows are well organized. The surface-defect concentration was less than 0.001 ML (monolayer) prior to irradiation. Several dark spots are newly generated after laser excitation, as seen in images (c) and (d). Each dark spot corresponds to a Si-atom vacancy; they are in the form of monovacancies (VM) and vacancy clusters (VC).[6] In image (c), the VC's may be classified into either vacancy strings (VS), in which adjacent Si_{up}'s are removed in one dimension along a Si chain, or vacancy islands (VI), where adjacent Si_{up}'s are removed in two dimensions across the chains. Examples of the structures are indicated by circles labeled S and I in image (c). Images (c) and (d) are acquired at the identical surface region but irradiated with a successively greater number of laser pulses, thus probing directly the modes of vacancy formation. In image (d), at the site enclosed by circles, labeled as *m*, the monovacancies are newly generated at originally perfect Si_{up} sites. Also in image (d), at the sites labeled as *c*, larger vacancy clusters form at sites nearest to pre-existing vacancies. Therefore, two different modes of bond rupture are induced by laser excitation on this surface.

To characterize the different modes of bond rupture, we statistically analyzed the images surveyed over 50 000 unit cells. In this analysis, we classified vacancies by size and morphology (VM, VS, and VI) as described above. Additionally we defined two quantities: the number density N_j and the vacancy-site density V_j of vacancy clusters consisting of $j(j\geqslant 1)$ vacancy sites.[7] The number density N_j is a count of vacancy clusters irrespective of their size. The site density V_j is the number *j* of vacant sites in an individual vacancy cluster. Figure 2(a) shows the number density of vacancy clusters, including VM (=V1), classified by their sizes, and Fig. 2(b) shows the number density classified by the defect morphology. They are plotted as a function of number of laser pulses. Figure 2(a) clearly indicates that VM's are generated predominantly at the early stage of irradiation and that larger clusters grow progressively at higher doses at the expense of VM's. The result reveals that vacancy formation takes place at individual surface sites successively and that bond rupture at the perfect sites is the primary step of this process. We emphasize that the efficiency of forming vacancy clusters is far above the value expected from the statistics of random formation of vacancies. Therefore, Si atoms near pre-existing vacancies show preferential removal.

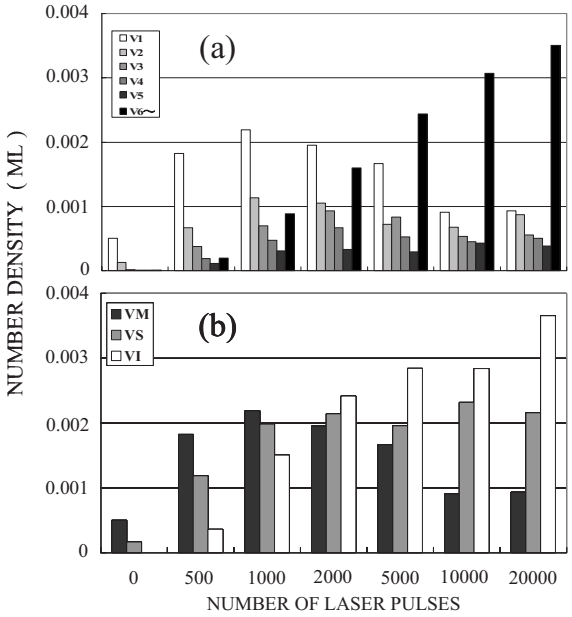

FIG. 2. (a) Growth of the number density of vacancy clusters classified with their sizes as a function of the number of laser pulses at a constant fluence of 30 mJ cm^{-2}. (b) Growth of the number density of monovacancies, vacancy strings, and vacancy islands as a function of number of laser pulses at a constant fluence of 30 mJ cm^{-2}.

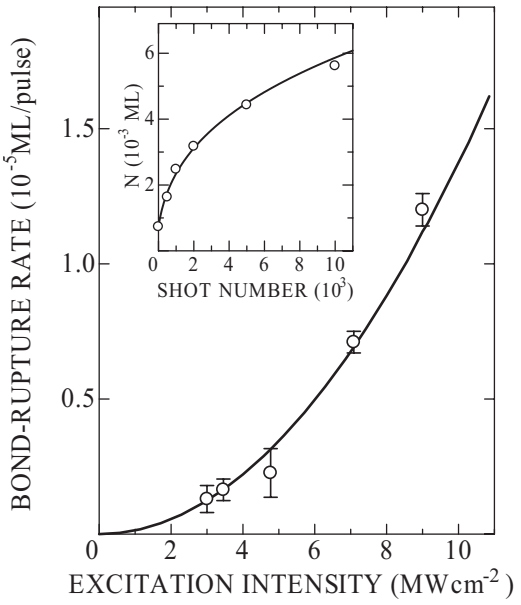

FIG. 3. The bond-rupture rate on surfaces with vacancy concentration less than 0.001 ML as a function of excitation intensity on the *n*-type Si(111)-(2×1) surface. The solid curve is the fit of the theoretical model derived by the two-hole localization mechanism (see text). The inset shows the growth of the total number density of Si vacancies on *n*-type surface excited at the intensity of 12.3 mJ cm^{-2} (3.5 MW cm^{-2}). The solid curve is the calculated result obtained by the theoretical model (see text).

Figure 2(b) shows the growth kinetics of the number densities for VM, VS, and VI. The predominant monovacancy formation at the early stage of irradiation is followed first by preferential generation of vacancy strings, and then by generation of vacancy islands at the expense of monovacancy and vacancy string formation. Therefore, the growth of vacancy clusters is anisotropic, and the efficiency of bond rupture at sites nearest pre-existing vacancies along the Si chain is higher than that across the chain.

Any bond ruptures at sites nearest to pre-existing vacancies enhance the total vacancy-site density $V(=\Sigma_j V_j)$ but do not change the total number density $N(=\Sigma_j N_j)$. Therefore, N represents the concentration of vacancies newly formed at originally perfect sites, free from any effects of vacancy formation near pre-existing defect sites. By analyzing N, we can quantitatively characterize the primary process of Si-bond rupture at originally perfect surface sites. In the inset of Fig. 3, we show the growth of N as a function laser pulse number n at a fluence of 12.3 mJ cm^{-2} on *n*-type surfaces. The increasing N up to about 0.5%, far above that on the surface prior to irradiation, provides additional evidence that Si_{up} atoms at intrinsic surface sites are subject to bond-rupture. We can evaluate the per pulse bond-rupture rate K_0 at the intrinsic sites from the slope of the growth curve N. The initial slope gives the value of 1.7×10^{-6} ML/pulse for the surface with a low defect concentration of 0.001 ML. This value is reduced to 2.7×10^{-7} ML/pulse after 5000 laser pulses where V is about 0.01 ML. Thus, the growth of N exhibits a decreasing rate with increasing dose, indicating the sensitive dependence of the bond-rupture rate on the surface-defect concentration. This decreasing rate is in contrast to the results from Si(111)-(7×7) surfaces, where the bond-rupture rate is constant up to a surface vacancy concentration of more than 0.05 ML.[4]

The process of surface vacancy formation was studied for several excitation intensities and different excitation wavelengths. First, growth curves of N were measured at different excitation intensities of 1064 nm laser pulses, and the rate of bond rupture at the intrinsic surface sites on the surfaces with vacancy concentration less than 0.001 ML was determined from the initial slope of the growth curve of N. Figure 3 shows the rate as a function of excitation intensity. It is clear that the rate depends superlinearly on the excitation intensity, similar to other semiconductor surfaces. The solid curve in the figure is calculated using the model described in the next section.

When the Si(111)-(2×1) surface is excited with nanosecond-laser pulses at different wavelengths, surface vacancy formation due to bond rupture of Si_{up} atoms was detected with spatial characteristics similar to those for 1064 nm excitation described previously. To demonstrate this similarity, number densities of VM, VS, and VI induced by 460 nm laser excitation are compared with those from 1064 nm excitation as a function of V (Fig. 4). For two different excitation wavelengths, fractions of vacancies in the form of monovacancy, vacancy strings, and vacancy islands are statistically equal. The result shows that the morphology of vacancy formation is not dependent on the excitation wavelength, thus suggesting a similar mechanism of bond rupture regardless of excitation wavelength. However, the rate of bond rupture depends on the excitation wavelength;

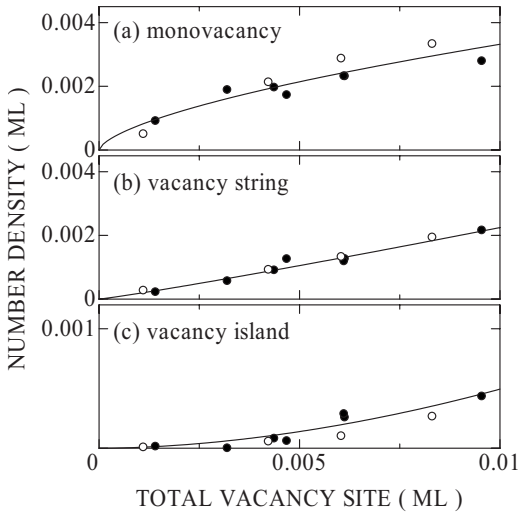

FIG. 4. The number density of (a) monovacancies, (b) vacancy strings, and (c) vacancy islands, as a function of total vacancy-site density excited with 460 nm (○) and 1064 nm (●) laser pulses at the same fluence of 25 mJ cm^{-2}.

the per pulse rate for 460 nm excitation is higher by a factor of 100 than that for 1064 nm excitation for the same fluence.

Finally, we compare the kinetics of vacancy formation on *n*-type and *p*-type surfaces to gain deeper understanding of the bond-rupture process. In Fig. 5, we show the growth of the total number density and total vacancy-site density of Si vacancies generated on surfaces of *n*- and *p*-type specimens. Excitation was made with 1064 nm laser pulses at a fluence of 10.5 mJ cm^{-2} for both specimens. The error bars in the figure represent the maximum estimated errors based on several series of similar measurements. It is clear that the growth of total number density is essentially the same for

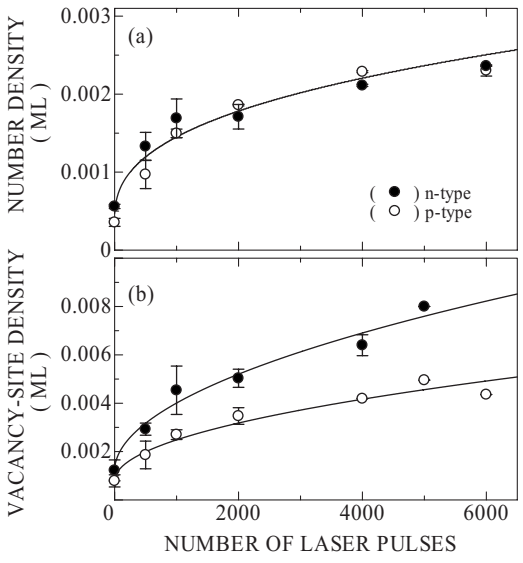

FIG. 5. (a) The growth of the total number density of Si vacancies on *n*-type (●) and *p*-type (○) surfaces excited at the same fluence of 10.5 mJ cm^{-2}. (b) The growth of total vacancy-site density of Si vacancies on *n*-type (●) and *p*-type (○) surfaces excited at the same fluence of 10.5 mJ cm^{-2}.

both surfaces. However, the total vacancy-site densities on *n*-type surfaces are significantly higher than that on *p*-type surfaces; bond rupture at sites nearest to pre-existing vacancies is enhanced significantly on *n*-type surfaces. Therefore, the position of the Fermi level plays an important role in the bond-rupture process, but only at sites near pre-existing vacancies.

IV. DISCUSSION

A. Electronic processes as the origin of surface bond rupture

As demonstrated in the preceding section, 1064 nm excitation induces bond rupture of threefold-coordinated Si atoms at intrinsic sites on Si(111)-(2×1). Since the effects of surface-specific optical transitions can be neglected around 1064 nm, the primary effect of 1064 nm light is bulk-valence excitation. Because of the small linear absorption coefficient (α=11 cm^{-1}) at this wavelength, free-carrier absorption and/or two-photon absorption may play some roles in the interaction. In fact, it has been shown that the threshold fluence F_{th} for Si surface melting strongly depends on the peak intensity or pulse width at 1064 nm.[21] Therefore, we first examine the possible effects of nonlinear optical processes under the present experimental conditions.

In bulk silicon, the two-photon absorption cross section β is 2 cm GW^{-1} at 1064 nm.[21,22] For the nanosecond-laser pulses used in the present study, the flux is less than 10 MW cm^{-2}, which leads to the two-photon absorption rate being less than that of the linear absorption by a factor of 1/1000. Therefore, we can completely neglect the two-photon absorption process. However, free carrier absorption becomes significant when the carrier density is more than 10^{19} cm^{-3}.[21,23] To clarify the effects of free-carrier absorption in the present case, we carried out a numerical simulation based on the model proposed by van Driel.[21] With parameters that reproduce well the experimental F_{th}'s for picosecond-laser pulses, we found that F_{th} is 4.2 J cm^{-2} for 3 ns pulses, being consistent with an extrapolated value of experimental results.[21] Numerical calculation also shows that the possible lattice temperature rise ΔT is only 0.2 K and that the electronic temperature T_e is only 0.4 K higher than the lattice temperature during the pulse. Therefore, free-carrier absorption also does not play a significant role under nanosecond-laser excitation at these intensities.

The important role of hot electrons has been demonstrated in the study of molecular desorption from metal surfaces under femtosecond-laser excitation.[24] However, this effect is usually absent for nanosecond-laser excitation that cannot result in high T_e.[24] The very low T_e, evaluated by taking possible effects of free-carrier absorption into account, excludes hot-electron effects as a mechanism for bond rupture on this Si surface. Also, we can completely neglect laser-induced heating effects based on the numerical simulation results. Since the (2×1) structure is stable up to 520 K,[12] a ΔT of less than 1 K from the base temperature (296 K) cannot contribute to any structural instability. Therefore, we conclude that the valence excitation with excess energy of as low as 0.05 eV is responsible for the bond rupture of Si

atoms on Si(111)-(2×1) by an electronic mechanism.

As described in Sec. III, laser-induced surface bond rupture is characterized by bond breaking at individual surface sites. Therefore, excited species generated in the bulk valence states must localize at a surface site to induce bond rupture. The dynamics of the carrier transfer and localization at surface sites are strongly influenced by band bending.[25] The Fermi level of Si(111)-(2×1) is pinned around 0.38 eV above the valence-band maximum (VBM) under thermal equilibrium,[12] leading to the band bending V_{S0}. The Fermi levels of the present n-type (p-type) specimens are located 0.88 eV (0.16 eV) above the VBM. Therefore, we have upward (downward) band bending of 0.50 eV (0.22 eV) for n-type (p-type) surfaces in thermal equilibrium.

The length of the depletion layer z_d is 4.82×10^{-5} cm (1.12×10^{-5} cm) for n-type (p-type) specimens, which is much shorter than the penetration depth of 1064 nm light. Therefore, laser excitation can change the band bending significantly, and the band becomes flat under intense excitation via the photovoltaic effect with surface photovoltage V_{SPV}. Based on the standard formula given in Ref. 12 and on the previous experimental results,[26] we can estimate the critical excess carrier density at which the surface photovoltage becomes equal to the surface band bending; the band becomes flat above this density. For a given excess carrier density N_C generated by incident light, V_{SPV} and V_{S0} satisfy the following relation:

$$\{\exp(\nu_{SPV})-1\}/\sqrt{\nu_{S0}-\nu_{SPV}}=N_C/N_n, \tag{1}$$

where $\nu_{SPV}=|V_{SPV}/k_BT|$ and $\nu_{S0}=|V_{S0}/k_BT|$, with the Boltzmann constant k_B. N_n is a factor for normalizing the density of excess carriers. Marsi *et al.* have shown that the surface photovoltage of 70 meV is induced at a carrier density of 2.8×10^{12} cm^{-3} for n-type Si(111)-(2×1).[26] Using Eq. (1), we estimate that the flatband condition is established for excess carrier densities greater than $N_c=1\times10^{15}$ cm^{-3}. As shown below, the laser-induced carrier densities in the present experimental condition are typically 10^{17} cm^{-3}. Therefore, the flatband condition is established at the onset of the nanosecond-laser pulse; most fractions of photogenerated carriers are governed by the flatband condition. This is an important condition under which we discuss the mechanism of surface bond rupture.

B. Two-hole localization mechanism

1. Qualitative features

As shown in Sec. III, the first feature of the excitation-induced structural instability on Si(111)-(2×1) is that the bond rupture at originally perfect individual sites is induced as the primary step. Therefore, an intrinsic mechanism of excitation localization is the key to the understanding of the overall mechanism. The second feature is that the bond-rupture rate depends superlinearly on the excitation intensity, as indicated in Fig. 3. Therefore, some nonlinear interaction among excited species plays a crucial role in the process. A few models have been proposed for the excitation-induced instability on semiconductor surfaces.[27–30] Among these models, we tentatively adopt the two-hole localization (THL) mechanism proposed by Sumi[29] as a working hypothesis, since it has satisfactorily described the characteristic features of the excitation-induced instability observed for other reconstructed semiconductor surfaces.[4,6,7,11] We discuss the instability on Si(111)-(2×1) in terms of the THL mechanism, first qualitatively, and then quantitatively by reformulating Sumi's theory to make it applicable to the present case. A critical discussion of alternative mechanisms will follow.

The primary mechanistic assumption in THL is that surface bond rupture leading to neutral-atomic desorption (not ion desorption) can be induced by strong lattice relaxations associated with localization of two valence holes on the same surface bond.[27,29] This assumption is based on the Anderson negative U concept that the localization of two carriers with the same charge is possible when strong lattice coupling results in favorable system energetics.[31] The negative U interaction of two-hole localized configurations may correspond to the displacement of surface atoms into the vacuum in the THL mechanism.

The THL mechanism assumes that the first hole is localized momentarily on a surface site. Although any valence excitation cannot be localized via intrinsic mechanisms in the bulk of Si crystals, the localization of holes at intrinsic surface sites of Si(111)-(2×1) is possible. First, the surface π band, composed of occupied Si_{up} dangling bonds, is almost degenerate with the VBM.[12] Then, the bulk-valence holes in the surface region can easily be scattered into the π band via electron-phonon and/or electron-electron scattering. This is supported by a time-resolved photoelectron spectroscopy study[25] that has revealed an effective injection of bulk-valence holes into the π band. Second, the π band shows a strong one-dimensional characteristic, with small stabilization energy due to delocalization and with strong electron-phonon interaction,[17,32] thus providing favorable energetics for localization. Third, localization of excited species upon any finite fluctuation of the lattice potential in a one-dimensional system has been predicted.[33] In fact, exciton localization has been predicted theoretically on this surface.[17] Therefore, localization of the holes injected into the π band at intrinsic surface sites is highly likely, as a consequence of the structural and electronic properties of this surface.

In the energetics of THL, the crucial physical quantities are the electron-lattice interaction S in the two-hole localized configuration, together with the Coulomb interaction energy U between two holes localized at the same bond, and the kinetic energy E_b lost in the process of localizing the second hole at the bond. In order to realize neutral-atomic desorption due to bond rupture by THL, these energies have to satisfy the following relationship:[29]

$$E_b+U-S\leqslant 0. \tag{2}$$

The kinetic energy loss E_b is estimated to be about 1.5 eV from the half-band width of the heavy-hole branch ($\sim$3 eV). Also, as shown below, U can be calculated to be about 1 eV on Si(111)-(2×1) by assuming the surface dielectric constant to be an average of the bulk and vacuum values. Although the electron-lattice interaction at the two-hole localized state on Si(111)-(2×1) is not reported, the

energy of about 2.5 eV has been suggested on GaP surfaces.[29] Since structural and electronic properties of Si(111)-(2×1) and GaP(110)-(1×1) are similar, we may presume a similar value for S of 2–3 eV on Si(111)-(2×1). Therefore, a crude estimation of energies suggests that THL mechanism can be applied to this surface.

As seen in Fig. 3, the bond-rupture rate at intrinsic surface sites shows a superlinear dependence on the excitation intensity. The rate of bond rupture due to THL, calculated by Sumi, inherently includes this superlinear dependence on the excitation density due to the quantum statistics of densely populated valence holes. Thus, qualitative discussions suggest that the THL mechanism is applicable to the electronic bond rupture on Si(111)-(2×1). In fact, this mechanism can quantitatively describe all important features of excitation-induced structural instability on this surface.

2. Quantitative analysis

a. Bond-rupture rate induced by two-hole localization of non-equilibrated valence holes. The rate of surface bond rupture J, due to successive two-hole localization, is given by

$$J = N_d R_{SHL}, \tag{3}$$

where N_d is the density of bonds localizing the first hole and R_{SHL} is the rate constant for localizing a second hole at the same bond.[29] For equilibrated valence-hole systems characterized by the Fermi energy E_F for holes, N_d of the first-hole localized metastable state with energy E_d ($E_d > E_F$) is approximated as

$$N_d = N_0 \exp\{-(E_d - E_F)/k_B T\}, \tag{4}$$

where N_0 represents the total density of bonds capable of holding the first localized hole. The rate constant R_{SHL} is given, for equilibrated valence holes, by

$$R_{SHL} \approx C \exp(E_F/k_B T), \tag{5}$$

where C is specific to the system under consideration, defined as

$$C = [4\pi/(\hbar^2 S k_B T)]^{1/2} \int [g(E)\exp\{-E/k_B T - (E_b + U - E)^2/(4Sk_B T)\}]dE. \tag{6}$$

In Eq. (6), the function $g(E)$ is a spectral function of the matrix elements for the transitions from a delocalized state to the two-hole localized state. Then, J is given by

$$J = J_0 N_0 \exp(2E_F/k_B T), \tag{7}$$

where $J_0 = C\exp(-E_d/k_B T)$. As seen in Eq. (7), J depends on the excitation density through the factor $\exp(2E_F/k_B T)$, which is superlinear with respect to the excitation density.

In real cases, however, dense laser-induced valence excitations are far from equilibrated and even strongly nonequilibrated due to efficient carrier diffusion driven by concentration and temperature gradients. Recently, the theory of THL has been extended for the nonequilibrated valence holes in semiconductors.[34] For completeness, we summarize briefly the essential points of the modification.

For nonequilibrated carriers, local valence-hole distributions for temporal domains longer than a few picoseconds have been characterized in terms of quasi-Fermi level Ψ_h and an effective temperature T^*.[21] Under the effective-mass approximation, the quasiequilibrium local hole concentration $N_h(\vec{r},t)$ at position $\vec{r}$ and time t of a three-dimensional valence system is given by

$$N_h(\vec{r},t) = \frac{2}{\sqrt{\pi}} Z_h(T^*) \int_0^\infty \frac{\sqrt{x}}{\exp\{x - \eta_h(\vec{r},t)\} + 1} dx, \tag{8}$$

where $Z_h(T^*)$ is the effective density of states for valence holes at T^* and η_h is the reduced quasi-Fermi level given by

$$\eta_h = \frac{E_V - \psi_h}{k_B T^*}. \tag{9}$$

The symbol E_V represents the energies of the VBM.

Based on the classical Boltzmann equation in the relaxation-time approximation for nonequilibrium thermodynamics, the electrical currents of carriers are governed by the gradients of quasi-Fermi levels and effective temperatures. The explicit expression of current $\vec{J}$ of pair concentration due to a strong Dember field has been derived.[21,34] However, in the excitation density regime of N_h less than Z_h, any density-dependent effects on carrier diffusion, on band-gap gradient, and on temperature gradients can be ignored for nanosecond-laser pulses. Then, the local density of holes is governed by the equation of particle balance, given by

$$\frac{\partial N_h(\vec{r},t)}{\partial t} - D\nabla^2 N_h(\vec{r},t) = G(\vec{r},t) - R(\vec{r},t), \tag{10}$$

where D is the classical ambipolar diffusion constant, and G and R are the pair generation and recombination rates, respectively. By solving Eq. (10) under appropriate boundary conditions, we can evaluate the density of valence holes in the subsurface layer $N_h(0,t)$, which corresponds to the hole density in Sumi's theory contributing to the two-hole localization on surface sites.

Under the presumption of local equilibrium, we can replace the Fermi energy, for an equilibrated electronic system, by the quasi-Fermi level for the density of valence holes in the subsurface layer, both of which are correlated with Eq. (8). Although no analytical expressions are possible for the Fermi integral in general cases, we can approximate it for the density range $N_h < Z_h$ by using Ehrenberg's expression, yielding $\exp(-\eta_h) = Z_h/N_h - 1/4$. Then, the bond-rupture rate for nonequilibrium valence holes in a moderate density range is given by

$$J(t) = J_0 \left\{ \frac{Z_h}{N_h(0,t)} - 0.25 \right\}^{-2}. \tag{11}$$

The experimentally determined value of per pulse rate K_0 of bond rupture is obtained by integrating $J(t)$ with respect to time:

$$K_0 = \int J(t)dt. \tag{12}$$

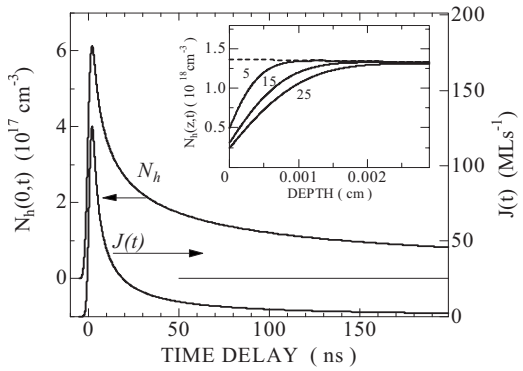

FIG. 6. The temporal change in hole density $N_h(0,t)$ near the surface generated by a 3.5 ns, 1064 nm laser pulse at the fluence of 32 mJ cm^{-2} and the bond-rupture rate $J(t)$ as a function of time, evaluated by the two-hole localization mechanism (see text). The inset shows the calculated spatial profiles of hole density from the surface generated by a 3.5 ns, 1064 nm laser pulse at the fluence of 32 mJ cm^{-2} on silicon for time delays of 5, 15, and 25 ns with respect to the peak of the incident pulse. The broken curve shows the concentration gradient without hole diffusion.

b. Numerical calculations and comparison with experimental results. Using the above equations, we calculate bond-rupture rates for comparison with measured rates. Since the laser-excited area is much wider than the area probed by STM, any effects of lateral carrier diffusion along the surface can be ignored. Then, the material balance equation is reduced essentially to a normal one-dimensional diffusion equation along a distance z from the surface. We use the following standard boundary conditions:

$$\lim_{z\to\infty} N_h(z,t) = n_i, \quad D \left.\frac{\partial N_h(z,t)}{\partial z}\right|_{z=0} = S_r N_h(0,t), \quad (13)$$

where S_r is the surface-recombination velocity and n_i is the hole density at thermal equilibrium which is negligible compared to laser-generated hole densities. We assume a Gaussian time profile of the laser pulse for $G(r,t)$ in Eq. (10) and consider only Auger recombination with the coefficient γ($=3.8\times10^{-31}$ cm^6/s) (Ref. 35) as a pair recombination rate, since the radiative recombination rate in Si is negligible for the present temporal domain. Thus, we can evaluate $N_h(z,t)$ with only one unknown parameter S_r.

The inset of Fig. 6 shows the spatial distributions of $N_h(z,t)$ with respect to the time of peak laser intensity, for some selected delays, at a laser fluence of 32 mJ cm^{-2}. Because of the small α at 1064 nm, holes are initially generated almost uniformly. However, surface recombination governed by S_r generates concentration gradients that induce hole diffusion toward the surface. In Fig. 6, we show the temporal evolution of the hole density near the surface, $N_h(0,t)$; it reaches the peak density of 6×10^{17} cm^{-3} at the end of a laser pulse followed by a slow decay. Because of the slow recombination rate in bulk Si and the persistent hole flow from the bulk, the hole density in the subsurface layer maintains relatively high density for a long time after nanosecond-pulse excitation. The bond-rupture rate at time t, evaluated by inserting $N_h(0,t)$ into Eq. (11), is also shown in Fig. 6. The bond-breaking process induced by a 3.5 ns pulse effectively lasts for a few tens of nanoseconds. The result of K_0, evaluated by integrating $J(t)$ with respect to time, is plotted (the solid curve) as a function of the excitation intensity in Fig. 3 and compared with experimental results. The calculated results fit the experimental data reasonably well. The magnitude of S_r used in the calculation is 1×10^4 cm s^{-1}. However, a rather wide range of S_r (5×10^3–8×10^4 cm s^{-1}) gave a similar nonlinear dependence.

In the evaluation of $K_0(I_{ex})$, we assumed $J_0=2.2\times10^3$ s^{-1} as fit from the absolute magnitude of the STM results. As an additional test of the theory, we evaluate J_0 based on Eq. (6). The exponent of the integrand in Eq. (6) exhibits a sharp peak with changing E at a particular energy E_T,[29] which represents an average kinetic energy of a free hole, with which it tunnels most dominantly to a bond at the first localized hole against the Coulomb repulsion between them. The energy E_T is given by

$$E_T = (2\pi k_B T S/\Delta)^{2/3} A^{1/3}, \quad (14)$$

with

$$\Delta = 2S - E_b - U + \frac{8}{3}\left(\frac{A}{U}\right)^{1/2}\frac{Sk_BT}{U} \quad (15)$$

and

$$A = e^4 m_h/(2\varepsilon_s^2\hbar^2), \quad (16)$$

where e is a unit charge, m_h is the effective mass of free holes, and ε_s is the static dielectric constant at the surface.[29] The values of the evaluated energies are listed in Table I, together with those obtained previously for GaP (Ref. 29) and InP.[36] The calculated J_0 ($=C$ for $E_d=0$) is 1.6×10^3 cm s^{-1} which is reasonably consistent with the value we used in evaluating K_0. Therefore, the THL theory reasonably describes both the superlinear dependence of the bond-rupture rate on I_{ex} and its absolute magnitude.

TABLE I. Several energies for the two-hole localization on Si(111)-(2×1) and (110) surfaces of GaP and InP, and the surface static dielectric constant (ε_s) and the effective mass of heavy hole (m_h). The m_0 is the rest mass of electron, and for symbols in the table, see the text.

	Si(111)-(2×1)	GaP[a]	InP[b]
E_d (eV)	0	0.5	0.77
E_b (eV)	1.5	1.0	1.2
U (eV)	1.0	1.0	0.83
S (eV)	2.5	2.5	2.75
E_T (eV)	0.14	0.16	0.13
ε_s	6.45	6	6.8
m_h	$0.49m_0$	$0.67m_0$	$0.45m_0$
C (s^{-1})	1.6×10^3	3.1×10^5	5.9×10^6

[a]Reference 29.
[b]Reference 36.

Next, we analyze the bond-rupture rate as a function of surface-defect concentration. As seen in the inset of Fig. 3, the bond-rupture rate at originally perfect surface sites depends on the concentration of surface vacancy sites. An initial rate obtained from the slope of 1.7×10^{-6} ML/pulse reduces to a slope of 2.7×10^{-7} ML/pulse after 5000 pulses, where the total surface-vacancy-site density (V) increases to 0.01 ML. We presume that the primary effect of surface vacancies on the valence holes is effective trapping near pre-existing defect sites, since surface defects break the translational symmetry and may introduce localized electronic levels within the band gap. It is possible that hole localization around pre-existing vacancies may serve to enhance bond breaking near defects, leading to efficient formation of vacancy clusters as observed experimentally. On the other hand, defect-assisted hole localization reduces, on the average, the density of valence holes in the near surface region. Because the factor $\exp(2\eta_h)$ is strongly dependent on $N(0,t)$, a small reduction of $N(0,t)$ could significantly decrease the magnitude of the bond-rupture rate K_0. Therefore, the result in the inset of Fig. 3 is qualitatively consistent with the THL mechanism.

Hole trapping by pre-existing vacancies can be modeled by introducing a vacancy-concentration dependent term in S_R, for damaged surfaces,

$$S_R(V) = S_0 + \sigma V. \tag{17}$$

The symbol σ represents the average trapping velocity per surface vacancy. In principle, the trapping velocity may depend on the size and form of vacancy clusters. For simplicity, we assumed that each vacancy site has the same average trapping velocity, characterized by σ. Based on the experimentally determined total vacancy-site densities V, we solve Eq. (10) with the $S_R(V)$ to have $N(0,t)$ for the surfaces with a given surface vacancy concentration. Then, the bond-rupture rate per pulse is evaluated. The result is shown by the solid curve in the inset of Fig. 3; it reasonably describes the growth curve of N, or the bond-rupture rate as a function of V. The magnitude of σ obtained by the fitting procedure is 3.7×10^{-8} cm^3 s^{-1}, which is larger, by more than a factor of 10^3, than the magnitude of S_0/N_0 (2.6×10^{-11} cm^3 s^{-1}) for a perfect surface. The large value may reflect an effective hole trapping near defect sites rather than the intrinsic recombination process mainly determined by intrinsic surface electronic states.

C. Bond rupture near vacancy sites: Anisotropic growth of vacancy clusters and Fermi-level effects

Figures 1 and 2 show that an efficient formation of vacancy clusters via consecutive bond rupture is an important feature of structural changes on this surface. The mode of vacancy-cluster growth is highly anisotropic given that vacancy string formation precedes vacancy island formation. The formation of VSs results from bond rupture of Si atoms nearest to monovacancies and/or strings along a chain, while the formation of VI needs bond rupture at the neighboring sites of VMs or VSs across the chain. The anisotropic growth of the two types of vacancy clusters indicates that the per pulse rate K_α along the chain is higher than the rate K_β across the chain.

TABLE II. Total number densities prior to laser irradiation, $N_{VM}(0)$, and the laser-induced increase in the total number density, ΔN_{total}, and the densities of monovacancy, ΔN_{VM}, dimer-vacancy strings ΔN_{VS_2}, and dimer-vacancy clusters, ΔN_{VI_2} on n- and p-type Si(111)-(2×1) surfaces irradiated by 1000 shots of laser pulses at the fluence of 10.5 mJ cm^{-2}.

		p type	n type
$N_{VM}(0)$	(10^{-4} ML)	5.8±2.0	3.6±0.13
ΔN_{total}	(10^{-4} ML)	8.4±0.06	8.3±1.5
ΔN_{VM}	(10^{-4} ML)	5.9±0.05	4.2±0.02
ΔN_{VS_2}	(10^{-4} ML)	1.2±0.4	2.4±0.3
ΔN_{VI_2}	(10^{-4} ML)	0.054±0.02	0.051±0.02
K_α/K_β		22±14	47±27
$2(K_\alpha+K_\beta)/K_0$		500±180	1400±260

To understand the microscopic mechanisms of the anisotropic growth of vacancy clusters and of enhanced rate of bond rupture at sites nearest to pre-existing vacancies, we quantitatively analyzed the vacancy-cluster growth process. To simplify the statistical analyses, we restricted ourselves to a particular dose region where monovacancies and vacancy clusters consisting of two adjacent vacancies dominate other higher aggregates. In this region, the density of VM increases by bond rupture at perfect sites with the rate K_0 but decreases by the bond rupture at the nearest sites to transform into VS_2 with the rate $2K_\alpha$ and VI_2 with the rate $2K_\beta$ (the factor of 2 comes from the available sites nearest to one VM). When we assume that the bond-rupture rates are constant in the limited dose region, then the number density N_{VM} of VM is governed by the following rate equation:

$$\frac{dN_{VM}}{dn} = K_0 - 2(K_\alpha + K_\beta)N_{VM}, \tag{18}$$

where the number n of laser shots is treated as a continuous variable for convenience.

Similarly, the number densities of VS_2 (N_{VS_2}) and VI_2 (N_{VI_2}) are given by

$$\frac{dN_{VS_2}}{dn} = 2K_\alpha N_{VM}, \quad \frac{dN_{VI_2}}{dn} = 2K_\beta N_{VM}. \tag{19}$$

Therefore, the ratio of K_α relative to K_β is obtained directly from the laser-induced number-density ratio of VS_2 relative to VI_2 after n laser pulses.

Table II summarizes the results of STM measurements for the surfaces irradiated by laser pulses with small doses, where the number densities of monovacancies and dimer vacancies are more than 80% of total number densities. Although the measured values are scattered statistically due to experimental difficulties in evaluating precisely the low-level defect concentrations, it is evident that ΔN_{VS_2} is substantially larger than ΔN_{VI_2} for both n- and p-type surfaces. The average ratio of K_α/K_β is 22 (47) for p-type (n-type) surfaces. Therefore, the rate along the chain is higher than that across

the chain, which is a primary reason why the vacancy strings are formed efficiently in low-dose regions.

Next, we compare the magnitudes of K_α (and K_β) relative to K_0. For low-dose regions, we may be able to approximate $2(K_\alpha+K_\beta)n \ll 1$ in Eq. (18). The ratio may then be estimated from the relationship obtained from the solution of Eq. (18):

$$\frac{2(K_\alpha+K_\beta)}{K_0} \approx \frac{1}{N_{VM}(0)}\left(1-\frac{\Delta N_{VM}}{\Delta N_{total}}\right). \tag{20}$$

The ratio $2(K_\alpha+K_\beta)/K_0$ evaluated from the results in Table II is about 500 (1400) for p-type (n-type) surfaces. Therefore, the bond-rupture rate at sites nearest to pre-existing monovacancies is strongly enhanced.

The aforementioned detailed measurements of atomic relaxation around a monovacancy have shown that the Si atoms near pre-existing vacancies are strongly relaxed. The occupied dangling bonds at the nearest sites of VM along the chain are displaced as much as 0.85 Å, while the displacement of the nearest site of a monovacancy across the Si chain is less than 0.3 Å.[37] The significant difference between K_α and K_β may be related to the strong anisotropy of relaxation of atoms around vacancies. The large distortions of surface atoms from their intrinsic sites can first contribute to enhancing the hole-trapping rate. Since carrier localization results from competition between intersite transfer and electron-phonon interaction at the site, the large displacement at a distorted site reduces the transfer and hence gives enough time to localize carriers via interaction with the lattice, leading to more efficient trapping of carriers. Also, strongly distorted atoms are generally in weakened-bond configurations due to reduced coordination and/or significant charge redistributions, which may enhance bond-rupture efficiency. Therefore, the atoms near pre-existing vacancies, in particular, along the Si chains, can have higher bond-breaking rates than normal sites upon successive two-hole localization.

With increasing dose, however, the number density of strings is saturated, and the saturation appears to be compensated by the efficient formation of vacancy islands as shown in Fig. 2. Therefore, bond breaking at the nearest sites across the chain becomes dominant in a high-dose region. The previous measurements have shown that the displacement of Si atoms nearest to a vacancy string consisting of three adjacent vacancies induces less displacement of the dangling bonds; the lateral displacement is only 0.3 Å along the $[0\bar{1}1]$ direction, almost the same as those at the nearest sites across the chains. Also, the number of nearest-neighbor sites on the neighboring chains increases with increasing vacancy string length, although the number of sites on the chain is always 2. These features may enhance bond breaking at the next chain, forming the vacancy islands instead of elongating vacancy strings.

There is another characteristic feature shown in Table II and Fig. 5(b), which is an interesting Fermi-level effect on the electronic bond rupture. It should be stressed here that the ratio $2(K_\alpha+K_\beta)/K_0$ on n-type surfaces and p-type surfaces are substantially different, far beyond statistical variation. Since the magnitude of K_0 (the rate of bond rupture at originally perfect sites) is the same for both n-type and p-type surfaces as shown in Fig. 5(a), this indicates that the rate of bond rupture at pre-existing defect sites is enhanced strongly on n-type surfaces relative to p-type surfaces

The enhanced rate of K_α relative to K_0 is more than a factor of 1000 on n-type specimens, implying that the lower density of holes can be active in rupturing bonds near defects, although they cannot induce bond rupture at perfect sites in a practical sense. As discussed before, the band becomes flat at the onset of the laser pulse. However, the photovoltaic effect is lost as the carrier density decreases. Therefore, spatial distributions of carriers at later time delays are affected again by the recovering band bending. Long *et al.* have shown that the recovery of the band bending to the original value takes a few microseconds.[38] Using numerical simulation, they demonstrated that the accumulation of valence-hole concentration near surface is induced at 1 μs after nanosecond-laser excitation and that the hole density accumulated is about one-tenth the initially populated hole density. Since the surface structures are different, we cannot directly apply this number. However, we may expect a similar effect for n-type Si(111)-(2×1). In the present hole-density regime, the bond-rupture rate is almost proportional to the square of the density. As we showed through numerical calculation, density near the surface region is typically 10^{17} cm^{-3} just after a nanosecond-laser pulse, which results in $K_0 \approx 1\times10^{-6}$ ML/pulse. Since K_α is 1400 times more efficient than K_0, the hole density of 10^{16} cm^{-3} can still be active in inducing bond rupture near defect sites. Therefore, on n-type surfaces, vacancy strings and clusters can be generated at late time delays after laser excitation. On the other hand, holes are repelled from the surface region of p-type specimens reducing the magnitude of K_α at late time delays relative to that on n-type specimens. Therefore, a strong enhancement of K_α particularly on n-type surfaces can be viewed as a direct consequence of the THL mechanism of bond rupture.

D. Possible roles of electrons and excitons in the laser-induced surface band rupture

We have discussed several features of laser-induced structural instability of Si(111)-(2×1) in terms of the THL mechanism. The characteristics of the instability are (1) superlinear dependence of the bond rapture rate on the excitation intensity, (2) efficient formation of vacancy clusters due to enhanced bond rupture near pre-existing vacancies, and (3) a prominent Fermi-level effect only on the bond rupture near vacancies. As shown above, the THL mechanism can describe the experimental results both qualitatively and quantitatively. In order to further substantiate the validity of the model, we briefly discuss the possible roles of other photogenerated excited species (electrons and excitons) in the surface bond-rupture process.

First, we discuss the roles of electrons in bulk conduction band and in the surface π^* band. As discussed before, the vibrational excitation mechanism of Si_{up} atoms by hot electrons can be ignored, since the electron temperature in the present case is too low. Since the electron is a fermion, a similar formalism can be applied for "two-electron localiza-

tion" for bond rupture: if two localized electrons could induce instability, electrons might localize in the unoccupied dangling-bond orbitals of Si_{down} atoms. Although no theoretical examination has been undertaken for localized electrons on semiconductor surfaces, it would be natural to suppose that the spatial extension of localized electrons is wider than that of localized holes. Therefore, structural instability due to two-electron localization, if any, may be weaker than that due to THL. Furthermore, as discussed above, the Fermi-level effects we observed clearly demonstrate that valence holes, not conduction electrons, play crucial roles in the Si-bond rupture at surfaces. Thus, we conclude that electrons generated by valence excitation are not active in inducing structural instability on Si(111)-(2×1). Rather, electrons injected in the surface π^* band may reduce the efficiency of the bond-rupture process through surface electron-hole recombination, which we considered only phenomenologically in terms of the surface-recombination velocity.

Rohlfing and Pollmann have shown theoretically that self-trapping of surface excitons on Si(111)-(2×1) is possible.[17] Although 1.15 eV photons induce bulk-valence excitation, electrons and holes transferred to surface π^* and π bands may lead to the formation of surface excitons that may eventually self-trap. In ionic crystals, exciton self-trapping is the primary mechanism of structural instability which results in lattice defect formation.[39] The instability in ionic crystals results from the repulsive interaction between an electron and a hole via electron-phonon interaction in deformable lattices, and during the self-trapping process, a few eV may be deposited into the lattice. However, the lattice relaxation energy of exciton self-trapping on the silicon surface is as small as 30 meV,[17] which is unlikely to break threefold-coordinated Si_{up} bonds. Multiexciton localization[30] could induce the instability to break the Si_{up} bonds, if exciton condensation were possible. However, since self-trapping is the intrinsic mechanism, localization of excitons may take place at intrinsic sites predominantly for surfaces with surface vacancy concentrations of less than 1%. Once the excitons are self-trapped, they are not mobile, so exciton condensation cannot be induced. On the other hand, we have revealed strong condensation of excited species responsible for the bond rupture around pre-existing vacancy sites; it implies that highly mobile excited species are responsible for bond rupture. Therefore, surface excitons cannot be the excited species responsible for the electronic bond rupture on this surface. We presume that radiative and/or nonradiative recombination, via self-trapping of excitons, may play a crucial role in surface electron-hole recombination, which can be the microscopic process responsible for the surface-recombination velocity.

V. CONCLUSION

We have shown that the laser-induced electronic bond rupture of Si atoms on the Si(111)-(2×1) surface is induced by the lowest bulk-valence excitation of Si. At the nearest-neighbor sites of vacancies, differences in the efficiency of bond rupture between *n*- and *p*-type surfaces indicate that bulk-valance holes in the surface region play the crucial role in the bond rupture. The THL mechanism of bond rupture gives a reasonable description, not only for the superlinear dependence of the bond-rupture rate but also for the decreasing rate of bond rupture as a function of vacancy density. Therefore, we have concluded that THL in the surface region is crucial for the excitation-induced bond rupture of Si atoms on the Si(111)-(2×1) surface.

ACKNOWLEDGMENT

This work was supported by a Grant-in-Aid for Scientific Research from the Ministry of Education, Science, Technology, Sports, and Culture of Japan.

[1] K. Ishikawa, J. Kanasaki, K. Tanimura, and Y. Nakai, Solid State Commun. **98**, 913 (1996).
[2] J. Xu, S. H. Overbury, and J. F. Wendelken, Phys. Rev. B **53**, R4245 (1996).
[3] X. H. Chen, J. C. Polanyi, and D. Rogers, Surf. Sci. **376**, 77 (1997).
[4] J. Kanasaki, T. Ishida, K. Ishikawa, and K. Tanimura, Phys. Rev. Lett. **80**, 4080 (1998).
[5] B. Y. Han, K. Nakayama, and J. H. Weaver, Phys. Rev. B **60**, 13846 (1999).
[6] E. Inami, K. Ishikawa, and K. Tanimura, Surf. Sci. Lett. **540**, L587 (2003).
[7] T. Gotoh, S. Kotake, K. Ishikawa, J. Kanasaki, and K. Tanimura, Phys. Rev. Lett. **93**, 117401 (2004).
[8] J. Kanasaki, A. Okano, K. Ishikawa, Y. Nakai, and N. Itoh, Phys. Rev. Lett. **70**, 2495 (1993).
[9] J. Kanasaki, K. Iwata, and K. Tanimura, Phys. Rev. Lett. **82**, 644 (1999).
[10] J. Kanasaki, N. Mikasa, and K. Tanimura, Phys. Rev. B **64**, 035414 (2001).
[11] J. Kanasaki, M. Nakamura, K. Ishikawa, and K. Tanimura, Phys. Rev. Lett. **89**, 257601 (2002).
[12] W. Monch, *Semiconductor Surfaces and Interfaces* (Springer, Berlin, 1995).
[13] K. C. Pandey, Phys. Rev. Lett. **47**, 1913 (1981); **49**, 223 (1982).
[14] P. Badziag and W. S. Verwoerd, Surf. Sci. **201**, 87 (1988).
[15] F. Ancilotto, W. Andreoni, A. Selloni, R. Car, and M. Parrinello, Phys. Rev. Lett. **65**, 3148 (1990).
[16] M. Rohlfing and S. G. Louie, Phys. Rev. Lett. **83**, 856 (1999).
[17] M. Rohlfing and J. Pollmann, Phys. Rev. Lett. **88**, 176801 (2002).
[18] G. Chiarotti, S. Nannarone, R. Pastore, and P. Chiaradia, Phys. Rev. B **4**, 3398 (1971).
[19] S. Selci, P. Chiaradia, F. Ciccacci, A. Cricenti, N. Sparvieri, and G. Chiarotti, Phys. Rev. B **31**, 4096 (1985).
[20] A. S. Grove, *Physics and Technology of Semiconductor Devices* (Wiley, New York, 1967).
[21] H. M. van Driel, Phys. Rev. B **35**, 8166 (1987).
[22] T. F. Boggess, Jr., K. M. Bohnert, K. Mansour, S. C. Moss, I. W.

Boyd, and A. L. Smirl, IEEE J. Quantum Electron. **QE-22**, 360 (1986).
[23] K. G. Svantesson, J. Phys. D **12**, 425 (1979).
[24] T. F. Heinz, M. M. T. Loy, and W. A. Thompson, Phys. Rev. Lett. **54**, 63 (1985).
[25] N. J. Halas, and J. Bokor, Phys. Rev. Lett. **62**, 1679 (1989).
[26] M. Marsi, M. E. Couprie, L. Nahon, D. Garazella, T. Hara, R. Bakker, M. Billardon, A. Delboulbe, G. Indlekofer, and A. Taleb-lbrahimi, Appl. Phys. Lett. **70**, 895 (1997).
[27] N. Itoh and T. Nakayama, Phys. Lett. **92A**, 471 (1982).
[28] A. Namiki, S. Cho, and K. Ichige, Jpn. J. Appl. Phys., Part 1 **26**, 39 (1987).
[29] H. Sumi, Surf. Sci. **248**, 382 (1991).
[30] O. Pankratov and M. Scheffler, Phys. Rev. Lett. **75**, 701 (1995).
[31] P. W. Anderson, Phys. Rev. Lett. **34**, 953 (1975).
[32] F. Ciccacci, S. Selci, G. Chiarotti, and P. Chiaradia, Phys. Rev. Lett. **56**, 2411 (1986).
[33] H. Sumi and A. Sumi, J. Phys. Soc. Jpn. **63**, 637 (1994).
[34] K. Tanimura, E. Inami, J. Kanasaki, and W. P. Hess, Phys. Rev. B **74**, 035337 (2006).
[35] J. Dwiezor and W. Schmid, Appl. Phys. Lett. **31**, 346 (1977).
[36] K. Tanimura, Phys. Rev. B **69**, 033301 (2004).
[37] E. Inami, K. Ishikawa, J. Kanasaki, and K. Tanimura, Surf. Sci. **528**, 115 (2003).
[38] J. P. Long, H. R. Sadeghi, J. C. Rife, and M. N. Kabler, Phys. Rev. Lett. **64**, 1158 (1990).
[39] A. K. S. Song and R. T. Williams, *Self-Trapped Excitons* (Springer, Berlin, 1993).